Annals of Materials Science & Engineering

Open Access

Austin Publishing Group

Research Article

Improved Fracture Toughened Epoxy Matrix System Reinforced with Recycled Milled Carbon Fibre

Cholake ST[1], Moran G[2], Joe B[1], Bai Y[3], Singh Raman RK[4], Zhao XL[3], Rizkalla S[5] and Bandyopadhyay S[1]*

[1]School of Material Science and Engineering, University of New South Wales, Australia

[2]Mark Wainwright Analytical Centre, University of New South Wales, Australia

[3]Department of Civil Engineering, Monash University, Australia

[4]Department of Mechanical and Aerospace Engineering and Chemical Engineering, Monash University, Australia

[5]Civil Engineering & Construction, North Carolina State University, USA

***Corresponding author:** Bandyopadhyay S, School of Materials Science & Engineering, University of New South Wales, Sydney, Australia

Received: July 13, 2015; **Accepted:** September 18, 2015; **Published:** September 20, 2015

Abstract

A stereology study of fracture surfaces of 1 to 10 wt. % short milled carbon fibre (SMCF) reinforced epoxy was carried out. Single edge notch bending (SENB) sharp crack samples over a fracture length of 10 mm, covering over 90 % fast crack growth, show that fibre – to – fibre distance significantly decreases with increased SMCF content. For 1% SMCF, the mean free path between fibres is 600 μm, whereas for 10 % SMCF, the mean free path is 110 μm, based on over 200 SEM images for each composition. In SENB sharp crack specimens tested at 2.8 mm/min, the slow crack growth region (length nearly zero for neat epoxy and maximum 1.14 mm for 10% SMCF-epoxy composite) shows intensive debonding and pull-out mechanisms. Fracture toughness (K_{IC}) increased from 0.78 $MPam^{1/2}$ for neat epoxy to 2.71 $MPam^{1/2}$ for 10 weight % SMCF/epoxy composites thanks to the combined effect of fibre stereology and the debonding/pull-out mechanisms. Notably, the flexural modulus of the 10 wt. % SMCF reinforced epoxy was 58 % higher than that of the neat epoxy.

Keywords: Fracture mechanics; Electron microscope; Polymers; Particulate filler; Reinforcement

Abbreviations

K_{IC}: Fracture Toughness; SENB: Single Edge Notch Bending; ESMCF XX: Epoxy Short Milled Carbon Fibre Series; CV: Coefficient of Variation; D_s: Inter-particle/Nearest Particle Distance; CFRP: Carbon Fibre Reinforced Plastic

Introduction

In recent years, epoxy is finding advantageous uses as a composite matrix in infrastructure applications [1-3]. But many times, the epoxy matrix fails to yield the required toughness (resistance to crack initiation and propagation) in the structure and hence many trials are undertaken to increase the fracture resistance of the epoxy. This has been attempted by adding second phase materials such as elastomers [4-6] and/or a rigid phase like alumina, silica or glass beads [7], which enhances fracture properties by a range of margins, however at a substantially increased material and processing cost and occasionally with reduction in modulus and or strength. A recent publication [8] using 3 weight % carbon nanotubes (CNT) in epoxy showed 17% improvement in fracture toughness (K_{IC}) of the epoxy and 48% improvement in K_{IC} of the composite laminate using 40% volume fraction CNT.

The present study aims to increase fracture property of the epoxy using cheap and commercially available recycled short milled carbon fibre (SMCF) without applying any surfactant or involving any additional mixing process- thereby keeping the fabrication cost of the modified epoxy matrix very low and at the same time obtaining a much tougher and stiffer modified epoxy.

The authors' earlier work [9] confirmed that the reinforcement SMCF a) does not interact chemically with epoxy and b) does not affect the curing time at room temperature.

Normally when epoxies cure, they undergo shrinkage of typically 3-7% which can impose a mechanical/physical compressive/squeezing force upon the filler. Subsequently during mode I testing, if the fillers undergo debonding from the epoxy interface and then separate through pull-out mechanism, the processes will be valuable energy absorbing sources [6].

Uniform dispersion and distribution of the reinforcement in the matrix are very important as well. If the distance between the fillers is small, and they are un-clustered and well distributed, then the

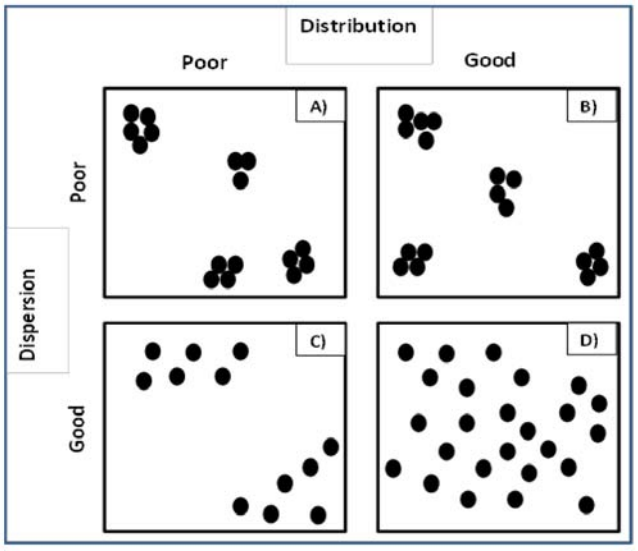

Figure 1: Various possible patterns of dispersion and distribution of fibres in the matrix: A) Poor distribution and dispersion; B) Good distribution but poor dispersion; C) Good dispersion but poor distribution; D) Good dispersion and good distribution.

Citation: Cholake ST, Moran G, Joe B, Bai Y, Singh Raman RK, et al. Improved Fracture Toughened Epoxy Matrix System Reinforced with Recycled Milled Carbon Fibre. Ann Materials Sci Eng. 2015; 2(2): 1023.

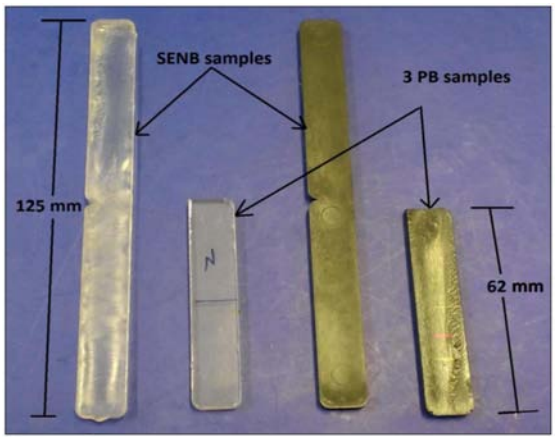

Figure 2: SENB and 3- point bending samples; two samples on the left are neat epoxy, and two samples on the right contain 3 wt. % SMCF.

fillers can act as more sites for arresting crack/micro-crack growth - implying that for cracks to re-start the system will have to go through multiple initiation stages (high energy absorbing) and subsequent propagation modes thereby enhancing the fracture properties of the modified epoxy [10]. Figure 1 provides a schematic diagram of the possible distribution features of fibre in matrix where the best and most even fibres scatter over the whole area (Figure 1D), providing optimum properties for crack arrest and reduction of subsequent initiation/propagation. This paper examines the uniformity of SMCF distribution in the epoxy matrix which is necessary for using the SMCF/epoxy system to generate future high quality continuous CFRP [11] systems. The inter-particle distance (D_s) of SMCF will naturally affect considerably the enhancement of the properties after fibre addition [12].

Materials and Methods

Materials

Commercial SMCF (MF100) supplied by ELG Carbon Fibre Ltd, had average diameter 7.5 µm, length 100 to 300 µm, and density 1.8 gm/cc as per information provided by the supplier. And a general purpose low shrinkage laminating epoxy system (EL-M) consisting of DGEBA and cyclo-aliphatic polyamine curing agent (hardener) was obtained from Barnes Pvt. Ltd, Sydney, Australia.

Sample fabrication

SMCF fibres were mixed with epoxy resin and stirred mechanically followed by 45 min ultrasonication after which hardener was added and stirred. The mixture was then allowed to cure at room temperature for 9 days in a silicon mould. The mould was casted in a way to produce Single Edge Notch Bending (SENB) samples having dimensions as per ASTM Standard D5045 [13] with an average notch length of 2.54 mm, as confirmed by a traveling microscope and a Vickers micro-hardness tester. Representative moulded samples are shown in Figure 2. The notch tip radius of the SENB samples was 0.25 mm as per the ASTM standard. Once the SENB samples were tested for fracture toughness, the separated parts were subsequently used as 3-point bending samples for measuring modulus of elasticity and flexural strength. The advantage of this procedure is that the same castings provide various properties, whilst maintaining the same material characteristics and dimensional requirements of ASTM D790 [14].

Table 1: Material designation showing wt. % and % volume fraction.

Material Designation	% Weight fraction of SMCF	% Volume fraction of SMCF
ESMCF 00	0	0
ESMCF 01	1	0.16
ESMCF 02	2	1.37
ESMCF 03	3	2.29
ESMCF 05	5	2.75
ESMCF 10	10	6.41

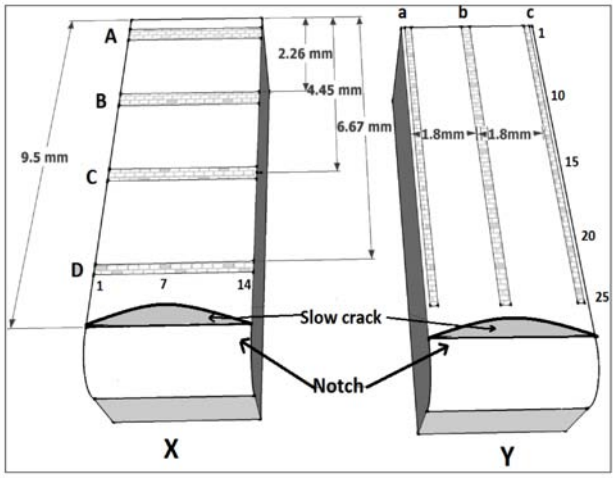

Figure 3: Schematic diagram of fracture surface of SENB samples showing location of SEM micrographs for determination of coefficient of variation. Crack direction is from bottom of the Figure to top. Numbers (1 to 14 in X and 1 to 25 in Y) imply the SEM images studied for stereology analysis.

In the results described below, epoxy/SMCF composites are designated as ESMCF 00 (neat epoxy), ESMCF 01, ESMCF 02, ESMCF 03, ESMCF 05 and ESMCF 10 representing the wt. % of SMCF added viz. 1, 2, 3, 5, and 10 %. The volume fractions were observed as 0, 0.16, 1.37, 2.29, 2.75 and 6.41% respectively as shown in Table 1.

SEM studies

A Hitachi tabletop TM 3000 scanning electron microscope (SEM) was used to study the fracture surfaces of the samples at different magnifications after the samples were gold coated using a Leica EM SCD050 coater. The gold coating was done at 60 mA current for 45 sec resulting in a15 nm thick coating.

Stereology

The distribution of the SMCF in the resin matrix is determined in terms of coefficient of variation (CV). For each composition3 samples were used, and each sample generated over 100(~60 in X direction and over 90 in Y direction) SEM images at 600X magnification (approximate 268 X 200 µm) taken at various places on the sample as shown schematically in Figure 3. From these observations the standard deviation and mean of the fibre population are calculated. The CV is the ratio of the standard deviation and the mean as determined by this procedure and is related to the variation in distribution. Lower CV values indicate better dispersion and usually CV close to 10% is considered as adequately uniform dispersion [15,16].

The same micrographs are used to determine inter-particle distance (D_s) using following equation 1 [12,17]:

$$D_s = 2d_p \frac{(1-V_p)}{3V_p} \quad \text{Equation 1}$$

where d_p is filler diameter (7.5 μm) and V_p is volume fraction which is taken as the ratio of the area covered by the number of fibresto the area covered by the total structure [18].

3-Point Bending Tests for flexural modulus and strength

Flexural strength and modulus of elasticity of the fabricated samples were determined in an INSTRON 5982 instrument using, as mentioned earlier, a 3-point bend test meeting ASTM D790 specification. The span length (S) was selected as 60 mm in order to maintain the span to depth ratio close to 16, to minimize the development of shear stresses in the sample [14]. The following equations were used to calculate flexural strength (σ_f) and modulus (E_f)

$$\sigma_f = \frac{3P_cS}{2BW^2} \quad \text{Equation 2}$$

$$E_f = \frac{S^3m}{4BW^3} \quad \text{Equation 3}$$

where P_c and m are maximum load and slope of the load-extension graph respectively, and B is the thickness of the sample with a width W. Average thickness of 3 point bend samples was 3.9±0.1 mm whereas the width was 12.5±0.5 mm, thereby maintaining W/B greater than 2 as a requirement for the plane-strain condition.

Fracture tests using single edge notch bending (SENB) specimens

Sharp notch (K_{IC}) crack driving force (fracture toughness/stress intensity factor) was calculated using the SENB test, at the Instron crosshead speed of 2.8 mm/min. and equation 4 [19].

$$K_{Ic} = \frac{P_cS}{BW^{3/2}}\left[2.9\left(\frac{a}{W}\right)^{1/2} - 4.6\left(\frac{a}{w}\right)^{3/2} + 21.8\left(\frac{a}{w}\right)^{5/2} - 37.6\left(\frac{a}{w}\right)^{7/2} + 38.7\left(\frac{a}{w}\right)^{9/2}\right]$$

Equation 4

In equation 4, *a* and W are crack depth and width of the sample respectively. A sharp crack was created by sliding the sharp razor blade over the notch tip making smooth continuous contact with the sample surface and keeping approximately constant force [20], the value of *a* after sharp crack being 2.8 mm (blunt crack + sharp crack). In the Results and discussion section K_{IC} is presented as a function of volume fraction of SMCF (V*f*).

Results and Discussion

Stereology

Dispersion and distribution: The stereology (dispersion and distribution) was undertaken, predominantly, in the fast crack growth region where debonding and pull-out is much lower compared to the slow crack region and the surface appears as flat/glassy under SEM. The findings are then related to the stereology at the crack initiation (slow crack) zone. Commonly, in the literature, stereology is done using saw-cut then polished samples. However, in composites debonding and pull-out are very valuable mechanisms, so in this stereology study, both fibre dispersion and the extent or lack of their debonding/pullout from beginning to end of the crack can be seen. SEM images in Figure 4 show no shear lips which confirms that the fracture (crack propagation) is in the plane strain condition [21] making the fracture surface suitable for stereology study.

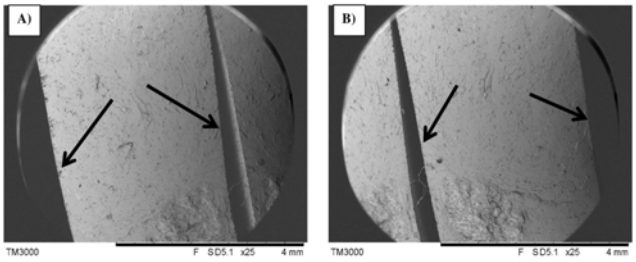

Figure 4: Sharp edges (no shear lips) observed in fractured test of ESMCF 03. Arrows in the Figure show edges of the samples.

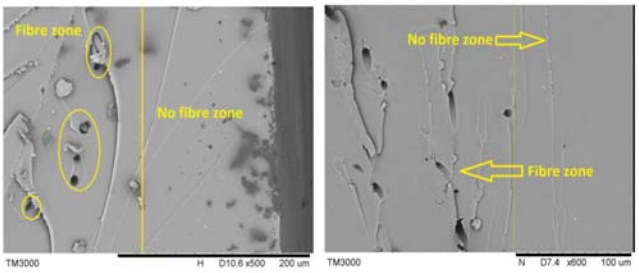

Figure 5: SEM images of ESMCF 01(left) and ESMCF 03 (right) at low and moderate magnification showing fracture surface near the edge.

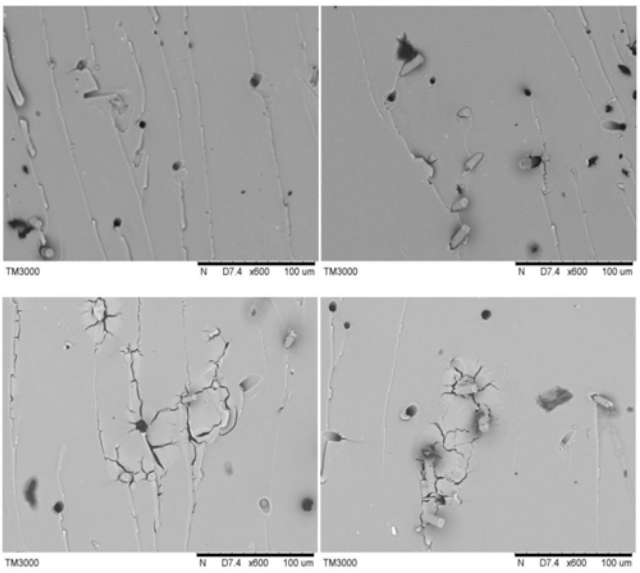

Figure 6A: SEM images of ESMCF 01 at moderate magnification away from the edge. Crack is propagating from bottom to top.

Figure 5 shows evidence of debonding and pull-out. It is also seen in Figure 5 that SMCFs are not present within a distance of 30-250μm from the sample edges which implies that the toughness of the epoxy has an important role. This distance from the edges was found to decrease as the SMCF wt. % increases. This is likely due to the fact that the attractive forces between epoxy and SMCF molecules are greater than that between air and SMCF [22]. In other words, it reveals the good wettability of SMCF by epoxy resin [22] which is an advantage.

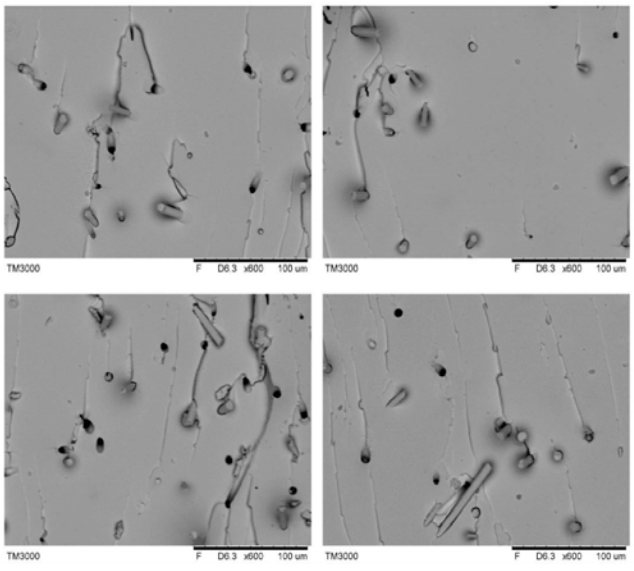

Figure 6B: SEM images of ESMCF 02 at moderate magnification away from the edge. Crack is propagating from bottom to top.

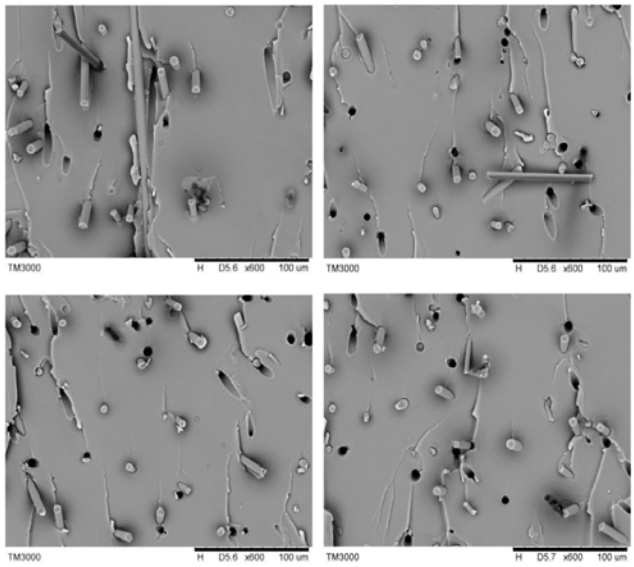

Figure 6D: SEM images of ESMCF 05 at moderate magnification away from the edge. Crack is propagating from bottom to top.

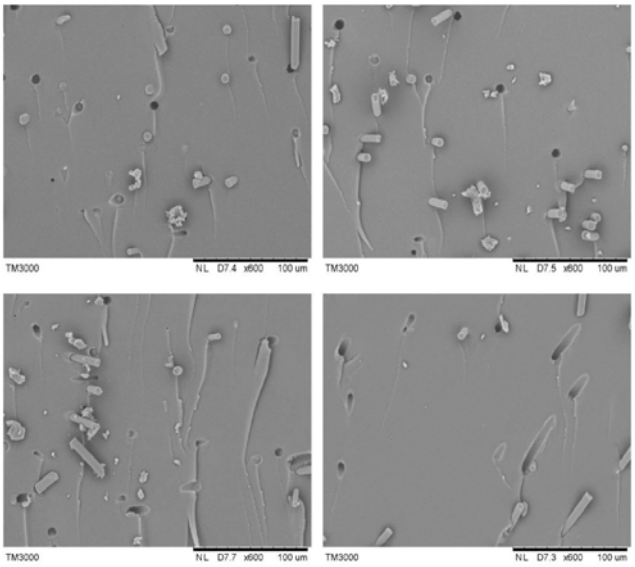

Figure 6C: SEM images of ESMCF 03 at moderate magnification away from the edge. Crack is propagating from bottom to top.

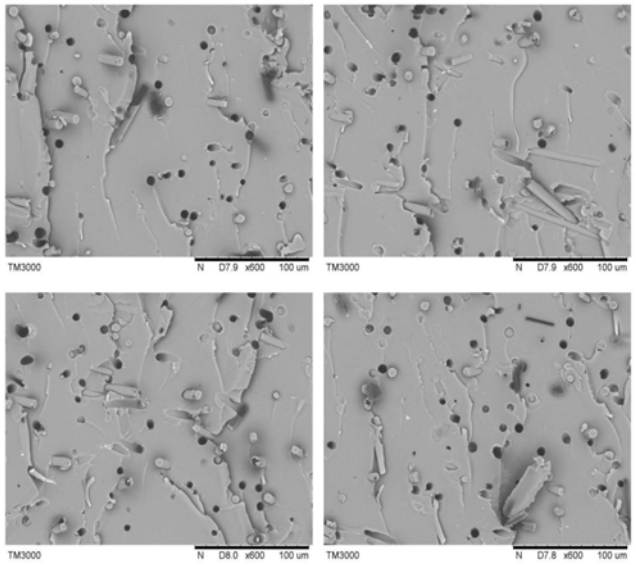

Figure 6E: SEM images of ESMCF 10 at moderate magnification away from the edge. Crack is propagating from bottom to top.

The same feature is observed on the bottom surface of the ESMCF series materials in contact with the mould and not exposed to air.

Figure 6A-E are selected SEM images at further higher magnifications, used for stereology analysis. To study the dispersion of SMCF, SEM images were taken from locations 300μm away from the edges (to study SMCF rich areas). It can be seen in Figure 6A-E that

a) The maximum numbers of fibres are aligned at angles between 45 – 90° (which is in the direction of the flow of epoxy while filling the mould) to fracture surface and

b) Very few fibres are observed parallel or 0 to 20° to the surface (i.e. perpendicular to flow). This benefit can be attributed to the ultra-sonication process.

c) This alignment of the fibres ensures the highest mechanical properties in the longitudinal direction.

With the help of SEM images (a limited number being shown in Fig.6 A-E for ESMCF01 upto ESMCF10), the standard deviation and mean number of SMCFs embedded in the epoxy matrix were determined in the X direction (perpendicular to crack propagation) and Y direction (parallel to crack propagation) - as illustrated in Figure 3 - and subsequently coefficients of variation (CV) were calculated to study the dispersion of the SMCF quantitatively in both X and Y directions. For Y axis distribution, as shown in Figure 3Y,

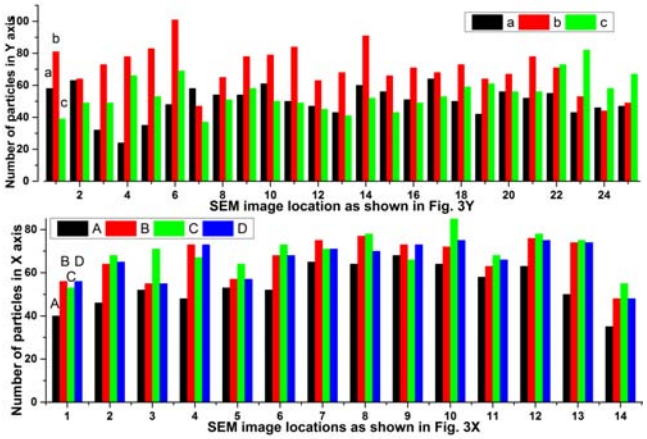

Figure 7: Observed number of SMCFs on the fracture surface of the ESMCF 10. Top graphs show average number of the SMCFs observed on locations a, b and c (Figure 3Y axis) whereas bottom graphs show strip A, B, C and D (Figure 3 X). Numbers on Y axis correspond to SEM image location as shown in Figure 3.

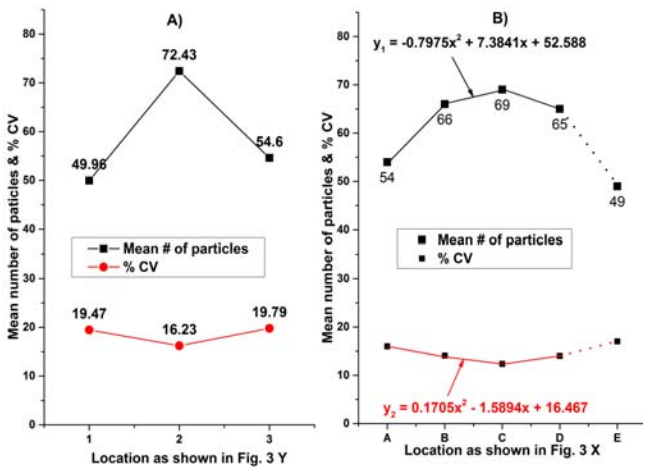

Figure 8: Average of four ESMCF 10 samples' mean number of SMCFs along with corresponding % CV in both directions A) 3Y and B) 3X axis.
Note: Lesser % CV shows more uniform distribution. In Figure B) Note: y_1 and y_2 represent mean number of SMCFs and % CV respectively and x indicates distance of the SMCFs from one edge of the sample which is opposite to the notch.

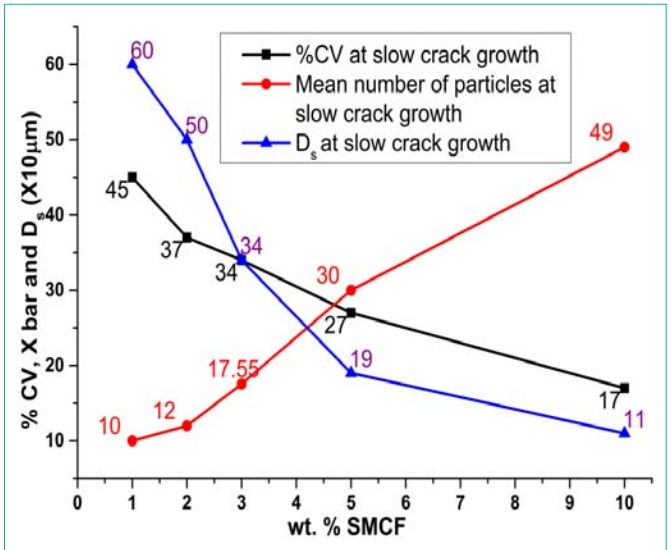

Figure 9: % CV and mean number of SMCFs per square at the slow crack/initiation region as a function of SMCF wt. %. Corresponding Ds (i.e. interparticle distance) is calculated using Equation 1.

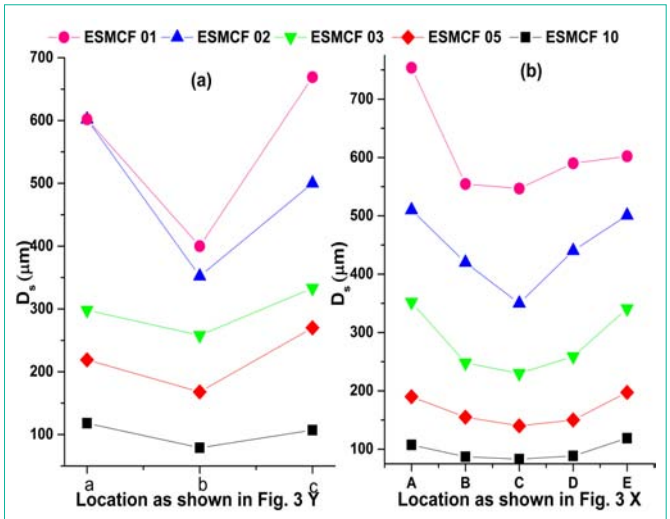

Figure 10: Inter-particle distance (D_s) calculated at different locations (same locations as above) in (a) Y and (b) X direction.

three stripes (named as a- bottom surface in contact with mould, b- centre and c- top surface) on the fracture surface were observed under SEM.

As shown in Figure 7 top, and Figure 8, the number of SMCFs at the centre stripe was a maximum and was low on both edges. Figure 8A shows that % CV was lowest at location b (Figure 3Y) indicating the better distribution of SMCFs at the core of sample than at both edges. Figure 7 bottom shows the number of SMCFs at locations A, B, C, D of Figure 3 X, and the mean number of SMCFs and % CV are reflected in Figure 8B.

To study the filler dispersion and distribution along the X axis, locations from A-D were selected as shown in Figure 3X where Stripe A was 300 μm away from the bottom edge (opposite to the notch), C the centre of the sample and B between stripes A and C. Stripe D is selected to be as close as possible to the slow crack growth region, but not entering the slow crack growth region. Again the number of SMCFs and % CV were respectively increasing and decreasing from the bottom edge (location A - in contact with the mould) to the centre (location C) and started decreasing toward the notch, as can be seen in Figure 8B).

The same observation was true for all ESMCF samples. Two polynomial equations in the form of $y=Ax^2+Bx+C$ (Figure 8B) are drawn for all samples expressing the most accurate relationship of mean number of SMCFs and % CV with the distance from the un-notched end of the sample. In this equation, A, B and C are constants (values are given in Figure 8B for ESMCF 10) and y_1 and y_2 represent mean number of SMCFs and % CV respectively and x indicates distance of the SMCFs from one edge of the sample which is opposite to the notch. The equations are subsequently used to find the mean number of SMCFs and % CV at the region where the crack is starting

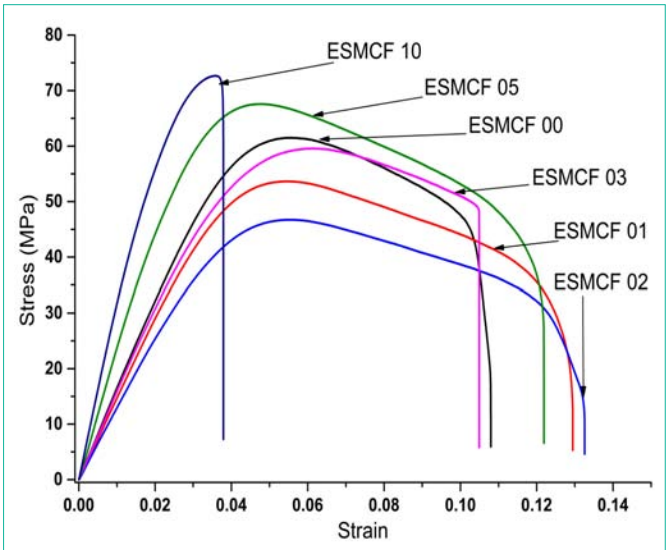

Figure 11: Flexural test Stress-Strain graph of ESMCF 00 (neat epoxy) and all epoxy-composite samples, after 9 days full curing.

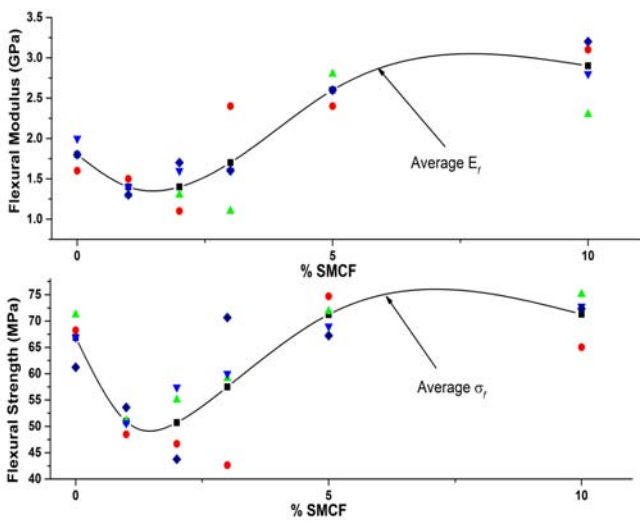

Figure 12: Variation in the flexural modulus (E_f) and strength (σ_f) on addition of various % of SMCF.

(slow crack) i.e. approximately where x = 9.8 mm. Other samples are also studied in the same manner to find the mean number of SMCFs and % CV at the slow crack growth/crack initiation zone and results are shown in Figure 9.

These results show that as SMCF doping increases, the % CV value decreases, which indicate an improved distribution of the fibres in the matrix at the sharp notch tip. The % CV calculated at different positions over the fracture surface of the sample had small variations especially at higher SMCF content (for ESMCF 05 and ESMCF 10, the % CV change observed was 7 and 5 % respectively). This suggests that SMCFs are well suspended and distributed in the epoxy resin matrix used; this is because of good wetting of SMCF by DGEBA epoxy resin. In addition to this, results obtained in the first part of this study back up this conclusion that high SMCF samples show less variation in densities (or apparently in % V_f) across small pieces of the same sample.

Figure 6A-E also reveal that SMCFs are not attracted to each other and do not form clusters, probably because of the slightly functionalised carbon on the surface of the fibres [9]. This proves that good dispersion and distribution (from low % CV) of SMCF in DGEBA epoxy resin (Figure 1D) is achieved without using any surfactant and/or advanced process of mixing, which would increase processing cost.

Inter-particle distance: Another parameter that affects the mechanical properties is inter-particle spacing which is a function of filler diameter and volume fraction [18]. Figure 6A–E show that though the SMCFs are well separated from each other, they are not equidistant, therefore the average inter-particle distance is determined using Equation 1. It is observed that as the volume fraction of filler material increases, average inter-particle/nearest neighbour distance (D_s) decreases. D_s at various zones studied as a function of content of SMCF is shown in Figure 10. For all samples D_s is higher at the edges because of fewer SMCFs, and is lower in the core area. Also it can be seen in Figure 10 that at higher dosage of SMCF i.e. 5 and 10 wt. %, small inter-particle distances are observed with less variation in D_s at

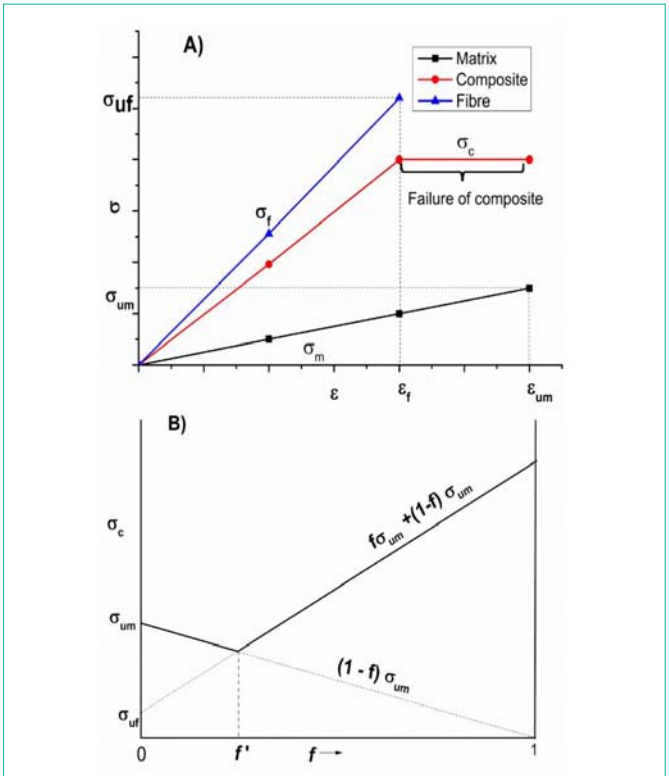

Figure 13: Rule of mixtures for the composite having $\varepsilon_{um} > \varepsilon_{uf}$. A) Stress strain behaviour and B) Composite stress as a function of fibre volume fraction.

the centre and edges, because of better distribution. With 10% SMCF, the average lowest distance between the nearest neighbors SMCFs observed was 0.09 mm (at Location C) which is significant enough to reinforce the continuous fibres such as carbon, graphite, glass or Kevlar in the ESMCF 10- epoxy matrix. D_s at location E (i.e. slow crack growth zone) in Figure 10(b) was calculated using the mean number of SMCFs values from Figure 9 which were determined from the equations shown in Figure 8. Further use of this D_S is explained

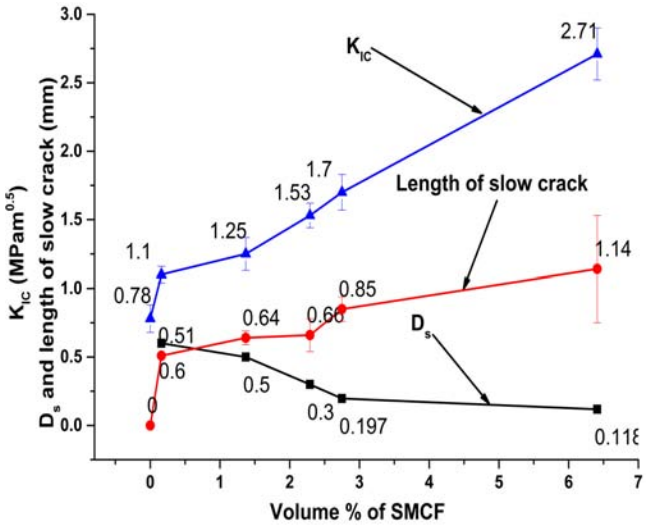

Figure 14: Change in notch fracture toughness (K_{IC}) of ESMCF series along with Ds as a function of volume fraction of SMCF.

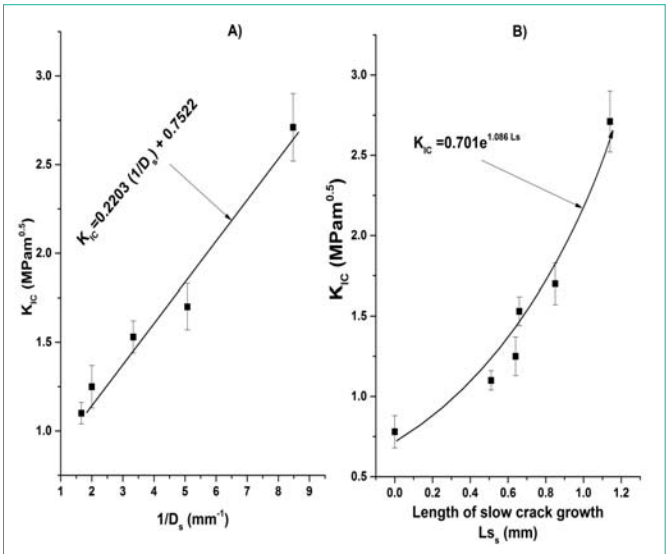

Figure 15: K_{IC} as a function of A) inverse of inter-particle distance ($1/D_s$) and B) length of slow crack zone (L_S).

in the next section.

3 point bending test for deformation and modulus testing: Figure 11 and Figure 12 show that addition of SMCF proves advantageous in improving flexural strength and modulus. But strain to failure calculated using failure extension does not show uniform change. This is because the fracture of a material vitally depends on the nature of initiation and propagation of the crack and small localised defects could eventually result in sudden failure of sample prior to actual value. Notably, the flexural modulus of the 10 wt. % SMCF reinforced epoxy was about 58 % higher than that of the neat epoxy. Also, the variations in strength are shown in Figure 12 which agrees with the conventional rule of mixtures as shown in Figure 13 [23,24].

Generally in particulate composites, ultimate strain in the matrix is greater than that of the filler ($\varepsilon_{um} > \varepsilon_{uf}$) (Figure 13 A for the present material) and the upper level of composite stress is given by the rule of mixtures [23,24], i.e., $\sigma_c = f.\sigma_f + (1 - f).\sigma_m$ till the strain reaches fibre failure i.e. ε_{uf}. Beyond this point, load starts transferring to the matrix. After failure, when the fibre aspect ratio becomes less than the critical aspect ratio, fibre does not bear load. Instead only matrix stress controls composite stress (Equation 5).

$$\sigma_c = (1 - f)\, \sigma_{mu} \qquad \text{Equation 5}$$

On the other hand, if the matrix fails while fibres are still bearing some load (when the aspect ratio is more than the critical aspect ratio) and composite stress becomes dependent on failure stresses of both matrix and fibre, the situation can be seen in Equation 6:

$$\sigma_c = f.\sigma_{uf} + (1 - f).\sigma_{um} \qquad \text{Equation 6}$$

Considering the above discussion, composite stress follows the rule of mixtures in case of $\varepsilon_{um} > \varepsilon_{uf}$, i.e. lower fibre volume fraction produces lower composite stress as predicted in theory (Figure 13, as created by the authors).

In particulate reinforced composites (such as the present systems), resulting composite strength mainly depends on the extent

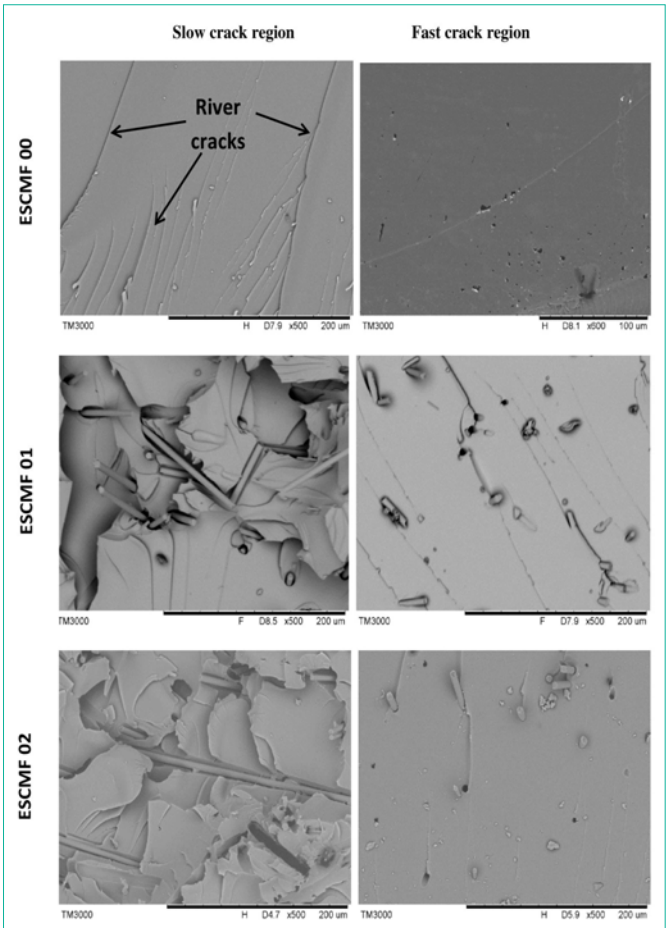

Figure 16 (continued): SEM images of fracture surface of ESMCF series in slow crack (left) and fast crack (right) growth region.

of load transfer from matrix to fibre [12]. At lower % SMCF, increased inter-particle distance and less uniform dispersion do result in poor transferring of applied load to SMCFs from the matrix, showing

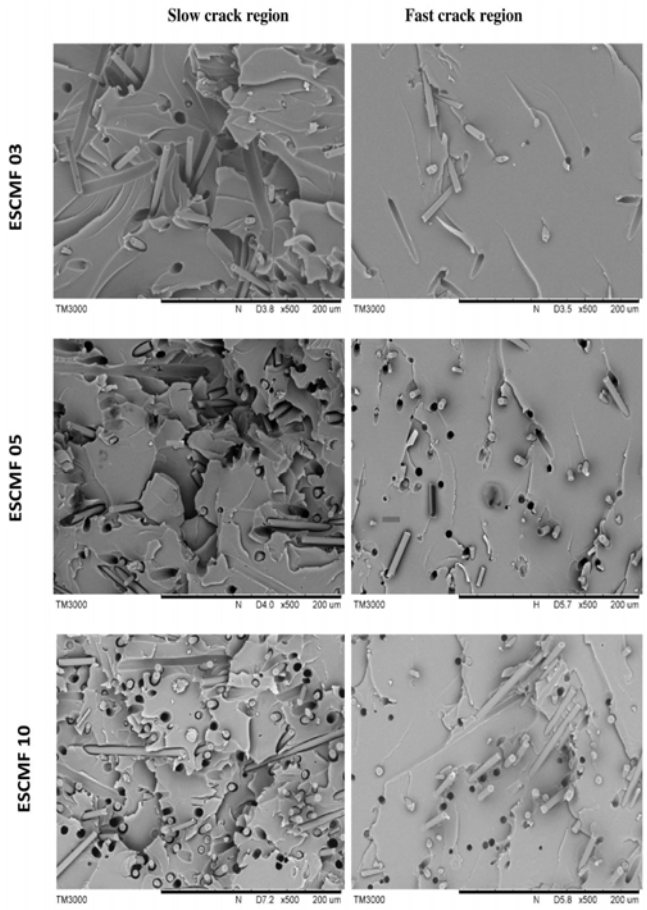

Figure 16: SEM images of fracture surface of ESMCF series in slow crack (left) and fast crack (right) growth region.

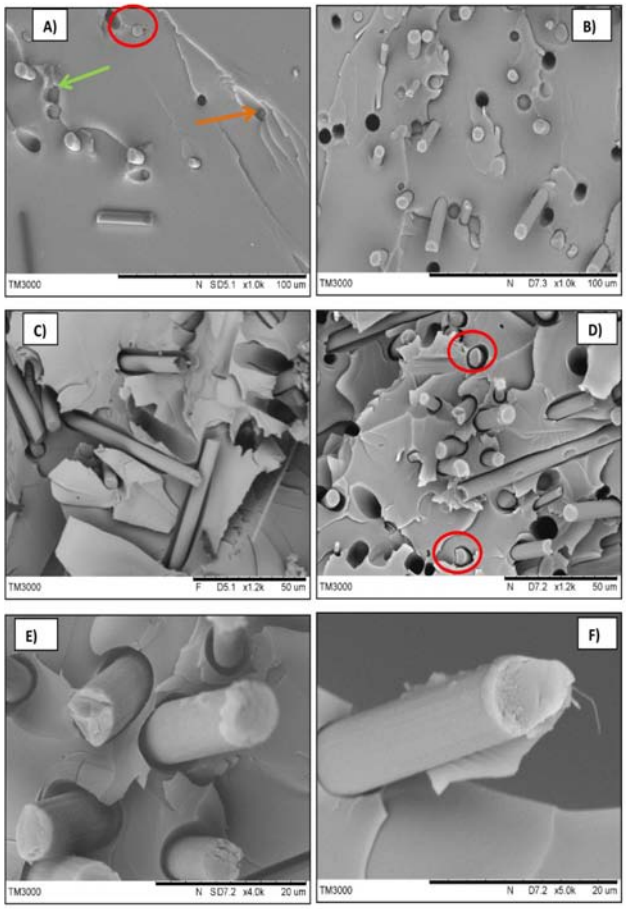

Figure 17: SEM images of crack propagation: A) ESMCF 03, B) ESMCF 10 show debonding and pull-out and crack pinning at lower magnification in fast crack growth region; C) and D) show similar features at higher magnification under slow crack growth i.e. crack initiation of ESMCF 05 and ESMCF 10. E and F) show still higher magnification views of fractured surfaces of SMCF in the slow crack region of ESMCF 10. In all SEM images, crack is propagating from bottom to top.

lesser composite strength. On the other hand, higher SMCF addition shows better dispersion of SMCFs in the resin matrix (e.g. ESMCF 05, 10), resulting in effective transfer of load and consequently improved strength. Higher loading of SMCF would result in a chain formation and a network due to tri-axial stresses around the fibres [10] which would transfer stress between fibres more effectively and show slight increase in strength. By contrast, this network is absent at smaller SMCF contents resulting in reduced strength because of stress concentration occurring around the SMCF segments (Figure 12) [25].

Cox [26] raised the issue of shear lag in composites with various lengths of discontinuous fibres. Raisanen [27] et al. in their experimental and modelling studies concluded that shear lag theory did not apply to random fibre networks as is the case of the present research.

SENB Fracture Tests: It is believed that the major disadvantage of epoxy resin is its poor resistance to crack growth [28] resulting in low fracture resistance properties. This has been overcome in this study by adding SMCF, as seen in Figure 14 which shows sharp (K_{IC}) notch stress intensity factor (fracture toughness) using the same specimen dimensions for the entire series of ESMCF materials. Figure 14 is industrially very attractive because of the fact that, with 10 % SMCF (6.4 V_f) addition in the epoxy, the fracture toughness goes up to 2.71 $MPam^{0.5}$ is which is literally 250 % superior compared to the neat resin. This can be related to the reduced inter-particle distance (D_s) of the SMCFs and length of slow crack growth (Figure 15A and B).

In Figure 15A, K_{IC} is observed to increase linearly with inverse of D_s. SMCFs act as obstacles to crack propagation and hence reduced inter-particle distance with good separation between neighboring SMCFs resulting in less nucleation defects because of greater interaction between tri-axial stress fields around the fibres. As can be seen in Figure 15A, for present system, the relation between K_{IC} and D_S can be expressed in term of a linear equation (K_{IC} = 0.2203[1/Ds] + 0.752) where 0.752 represents the K_{IC} of neat epoxy; Note K_{IC} is in $MPam^{0.5}$ and D_s is in mm.

Fractography: Figure 16 presents SEM fracture surfaces showing a)individual de-bonding and pull-out mechanisms during crack initiation i.e. slow crack growth which absorbs highest energy during the fracture process and b) fast crack growth i.e. crack propagation which involves much less energy [29,30]. The length of the slow crack growth region (L_S) was observed to increase with the SMCF wt. %

(Figure 14) and hence shows an exponential increase in K_{IC} (Figure 15B). These mechanisms are absent in ESMCF 00which shows only some river lines indicating brittle fracture as can be seen in Figure 16 A. De-bonding and pull-out are observed (Figure 16B to F) in slow crack growth, because of the optimum bond that may exist in the material for producing the pull-out of the fibres [29]. Another possible reason given by other researchers is the high strength of SMCF and the short bond length of SMCF which is its fibre length (100-300 μm) [31], whilst stress concentration gives rise to tri-axial stress around the filler which leads to de-bonding [10]. In addition to fibre pull-out, the rather small number of broken fibre sites (Figure 17A, shown by red circles) can act as sites for stress-triaxiality and thus induce crack initiation by de-bonding. These processes progressively extend the slow crack growth region and ultimately raises crack-resistance (K_R) [6,32].

After de-bonding, subsequent work of fracture depends on elastic energy in the fibre, surface energy of newly created interface and work of fibre pull-out that depends on the diameter of fibre, frictional shear as well as length of pull-out [30,33]. Individual de-bonding is observed in the ESMCF series which results in more newly created surface than bundle de-bonding, hence absorbing more energy [30]. At the same time debonding results in voids which alter the stress state in the matrix surrounding the voids. This leads to shear failure (Figure 17A shown by orange arrow) that absorbs excess energy for failure [10].

Crack pinning mechanism by the SMCFs was also observed on the fracture surface of the EMSCF system, as can be seen in Figure 17 (shown by yellow arrows in A and B). This is due to the differences between elastic properties of epoxy and SMCFs which results in SMCFs acting as stress concentration sites. This mechanism usually occurs when the propagating crack is impeded by rigid impenetrable well-bonded fibres [34]. The pinned crack tends to bow out between the SMCFs forming a secondary crack. Thus a new crack front is increased because of the changed shape between the pinning positions. After the new crack is initiated, energy is required not only to create the new fracture surface, but by analogy with the theory of dislocations, energy must also be supplied to the newly formed non-linear crack front, which is assumed to possess line energy and hence enhance the crack resistance [35]. The fractographic study shown in Figure 17 provides strong evidence that a crack pinning mechanism due to SMCFs incorporation is an effective reason behind the improved fracture toughness in the SMCF modified epoxy.

The broken surfaces of SMCFs shown in Figure 17E and F not only prove the participation of SMCF in the fracture mechanism but also they indicate good physico-mechanical bonding between the fibres (which are embedded in epoxy on other fracture side and appear as holes) and the epoxy.

Conclusions

1. This research uses fracture surfaces of single edge notch samples to study the stereology of SMCF in epoxy. It is demonstrated that for higher SMCF content, SMCFs are distributed uniformly without clusters, thereby resulting in good distribution and dispersion of fibres in epoxy.

2. The average inter-particle distance at the crack initiation zone was calculated using the equation established from the distribution geometry of SMCFs over the rest of the area. For the maximum weight % of SMCF used (10 %) the lowest average inter-particle distance was 110 μm which makes the SMCF modified epoxy an attractive matrix for addition of continuous fibre for infrastructural composites, considering that this is achieved without use of any surfactant.

3. Optimum mechanical bonding between SMCF and epoxy matrix improves the flexural strength and modulus.

4. It will be of industrial importance that for the 10 % SMCF (6.4 % V_f) – epoxy system the fracture stress intensity factors (K_{IC}) were typically 250 % superior to that of the neat resin. This increase was observed as a function of inter-particule distance and length of maximum energy absorbing region in the fracture mechanism i.e. slow crack growth region. The maximum energy absorbing nature of slow crack growth was found to be the result of the various mechanisms in ESMCF system including

- De-bonding and pull-out that results in a) more newly created surface, hence more surface energy absorption, b) voids which alter the stress state in the host matrix resulting in shear failure.

- Crack pinning mechanism resulting in enhanced crack resistance because of extra energy supplied to the newly formed non-linear crack front.

5. Fibre participation in energy absorption was also seen in fast fracture regions.

Acknowledgement

This research is sponsored by the Australian Research Council through the ARC Discovery Scheme under the project DP120101708 involving UNSW Australia, Monash University Australia and North Carolina State University USA.

References

1. Myers JJ. External Strengthening of Structures using Fibre-Reinforced Polymer Composites. In: Durability of Composites for Civil Structural Applications. Vistasp Karbhari, Editor. Wood head Publishing Limited: Cambs, England. 2007; 247-283.

2. Hollaway LC. A review of the present and future utilization of FRP composites in the civil infrastructure with reference to their important in-service properties. Constr Build Mater. 2010. 24: 2419-2445.

3. Dawood M, Rizkalla S. Environmental durability of a CFRP system for strengthening steel structures. Constr Build Mater. 2010; 24: 1682-1689.

4. Salmon S, Swank M, Ram GDJ, Stucker BE, Palmer JA. Effectiveness of epoxy staking of fasteners in aerospace applications. Assembly Automation. 2009; 29: 341-347.

5. Riccardi CC, Adabbo HE, Williams RJJ. Curing reaction of epoxy resins with diamines. J Appl Polym Sci. 1984; 29: 2481-2492.

6. Bandyopadhyay S. Review of the microscopic and macroscopic aspects of fracture of unmodified and modified epoxy resins. Mater Sci Eng A. 1990; 125: 157-184.

7. Bhatnagar MS. Epoxy Resin (Overview). In: The polymeric material Encyclopedia. 1996.

8. Mirjalili V, Ramachandramoorthy R, Hubert P. Enhancement of fracture toughness of carbon fibre laminated composites using multi wall carbon nanotubes. Carbon. 2014; 79: 413-423.

9. Cholake ST, Moran G, Bai Y, Singh Raman RK, XL Zhao, Rizkalla S, et al. Physico-chemical Characterization of Novel Epoxy Matrix System Reinforced

with Recycled Short Milled Carbon. J Miner Mater Characterization Eng. 2015; 3.

10. Fouchal F, Knight JAG, Dickens P, and Garrington N. On-line monitoring of epoxy resin cure using infrared, in 12th Solid freeform fabrication symposium. 2001; 441-451.

11. Fischer-Cripps AC. A simple phenomenological approach to nanoindentation creep. Mater Sci Eng A. 2004; 385: 74-82.

12. Shao-Yun Fu, Feng X, Lauke B, M MY. Effect of particle size, particle/matrix interface adhesion and particle loading on mechanical properties of particulate-polymer composite. Compos. B: Eng. 2008; 39: 993-961.

13. ASTM D5045-99. Standard Test Methods for Plane-Strain Fracture Toughness and Strain Energy Release Rate of Plastic Materials. ASTM international: West Conshohocken. 1999; 9.

14. ASTM D790-02. Standard Test Methods for Flexural Properties of Unreinforced and Reinforced Plastics and Electrical Insulating Materials. ASTM International: West Conshohocken. 2002; 9.

15. Kucharski S, Jarzabek D. Depth Dependence of Nanoindentation Pile-Up Patterns in Copper Single Crystals. Metall Mater Trans A. 2014; 45: 4997-5008.

16. Ma Z, Long S, Pan Y, Zhou Y. Creep behavior and its influence on the mechanics of electrodeposited nickel films. J Mater Sci Technol. 2009; 25: 90.

17. Young RJ, Beaumont PWR. Failure of brittle polymers by slow crack growth. J Mater Sci. 1975; 10: 1343-1350.

18. Atlas of Stress-strain Curves. 2nd edn. ASM International. 2002.

19. Broek D. Elementary Engineering Fracture Mechanics. 4th edn. Netherlands: Martinus Nijhoff Publishers. 1986.

20. Gong S, Bandyopadhyay S. Fracture Properties and Fracture Surface Morphologies in Rubber-PMMA Composites. J Mater Eng Perform. 2007; 16: 607-613.

21. Lucas GF, McKeighan PC, Ransom JS. Nontraditional methods of sensing stress, strain, and damage in materials and structures. West Conshohocken, PA: ASTM. 2001.

22. Noort RV, Barbour M. Introduction to dental materials. 4th edn. New York: Edinburgh. 2013.

23. Harris B. Engineering Composite Materials. 2nd edn. London: IOM. 1999.

24. Chamis CC, Sinclair JH. Prediction of Properties of Intraply Hybrid Composites. In Thirty fourth Annual Conference of the SPI Reinforced Plastics/composites Institute. New Orleans Louisiana. 1979; 19.

25. Guth E. Theory of Filler Reinforcement. J Appl Phys. 1945; 16: 20-25.

26. Cox HL. The elasticity and strength of paper and other fibrous materials. British Journal of Applied Physics. 1952; 3: 72-79.

27. Räisänen VI, Alava MJ, Niskanen KJ, Nieminen RM. Does the shear-lag model apply to random fibre networks? J Mater Res. 2011; 12: 2725-2732.

28. Moloney AC, Kausch HH, Kaiser T, Beer HR. Parameters determining the strength and toughness of particulate filled epoxide resins. J Mater Sci. 1987; 22: 381-393.

29. Bandyopadhyay S. Macroscopic Fracture Bahavior - Correlation with Microscopic Aspects of Deformation in Toughened Epoxies. In: Toughened Plastic I, Riew CK, Kinloch AJ, Editors. American Chemical Society USA. 1993.

30. Bandyopadhyay S, Gellert EP, Silva VM, Underwood JH. Microscopic Aspects of Failure and Fracture in Cross-Ply Fibre Reinforced Composite Laminates. J Compos Mater. 1989; 23: 1216-1231.

31. Wu C, Feng P, Bai Y, Lu Y. Epoxy Enhanced by Recycled Milled Carbon Fibres in Adhesively-Bonded CFRP for Structural Strengthening. Polym. 2013; 6: 76-92.

32. Low IM, Mai YW, Bandyopadhyay S, Silva VM. New toughened-hybrid epoxies. Mater Forum. 1987; 10: 6.

33. Kinloch AJ, Maxwell DL, Young RJ. The Fracture of Hybrid-Particulate Composites. J Mater Sci. 1985; 20: 4169-4184.

34. Lange FF. The interaction of a crack front with a second-phase dispersion. Philos Mag. 1970; 22: 11.

35. Kinloch AJ, Maxwell D, Young RJ. Micromechanisms of crack propagation in hybrid-particulate composites. J Mater Sci Lett. 1985; 4: 1276-1279.

Ann Materials Sci Eng - Volume 2 Issue 2 - 2015
ISSN : 2471-0245 | www.austinpublishinggroup.com

Citation: Cholake ST, Moran G, Joe B, Bai Y, Singh Raman RK, et al. Improved Fracture Toughened Epoxy Matrix System Reinforced with Recycled Milled Carbon Fibre. Ann Materials Sci Eng. 2015; 2(2): 1023.